Journal of Manufacturing Processes 43 (2019) 54–62

Contents lists available at ScienceDirect

Journal of Manufacturing Processes

journal homepage: www.elsevier.com/locate/manpro

Identification of optimal machining parameters in trochoidal milling of Inconel 718 for minimal force and tool wear and investigation of corresponding effects on machining affected zone depth☆

Abram Pleta*, Gouthaman Nithyanand, Farbod Akhavan Niaki, Laine Mears

Clemson University International Center for Automotive Research, 4 Research Drive, Greenville, SC 29607, USA

ARTICLE INFO

Keywords:
Trochoidal milling
Force modeling
Taguchi
Inconel
Milling
Machining affected zone
SEM

ABSTRACT

Increasing the productivity and efficiency of milling practices is of high importance with the rapidly changing global economy. To this end researchers have turned to alternative milling toolpaths, such as trochoidal milling, which has been shown to increase tool life with a corresponding reduction in machining time for some applications. To better understand the trochoidal milling process and optimize it for manufacturing scenarios, the modeling of cutting forces must be investigated; semi-mechanistic methods are the focus of this work. The basis for this type of force modeling lies in uncut chip thickness modeling combined with cutting force coefficients and edge force coefficients. With a novel uncut chip thickness model proposed by the authors in a previous work, this investigation looks to understand the dependence of the model coefficients as they relate to trochoidal path parameters along with machining outputs such as maximum cutting force and tool wear. Furthermore, the machining parameters are investigated as to how they relate to the improvement of tool life and cutting force utilizing the Taguchi method, where optimal parameters are found for minimum tool wear and cutting forces. The effects of the trochoidal path on the subsurface of the machined samples as they relate to the machining affected zone, are also investigated in both the radial and axial directions. It is found that tool wear increases the depth of the machining affected zone as does increasing chip thickness.

1. Introduction

Material removal processes to achieve desired geometries have long been followed in many industries such as aeronautical, automotive, and commercial products manufacturing. Milling is a key process in material removal due its robustness and ability to realize complex geometries. Milling has evolved over the years in terms of machines used and the cutting capabilities of tools. Optimization and improvement of different machining processes has been one continuing area of prime concern. Such improvements have been done for milling process as well, for many standard tool paths [1,2]. However, the use of alternative tool paths such as trochoidal milling to improve the process in terms of production time and cost have remained a clear research topic with the potential to realize greater industrial implementation [3]. Trochoidal milling has been proven to increase tool life and productivity [2]. Akhavan Niaki et al. proposed a numerical method of chip thickness model in trochoidal milling and compared the simulation and experimental force values to validate their model [3,4]. Thus, a study on optimization of trochoidal milling for minimum cutting forces and tool wear could serve to bridge the gap between industry and academia, as this could help to identify the optimal mathematical parameters that could be used in industry to implement trochoidal milling effectively.

The Taguchi method is developed to minimize the cost and time of finding optimized production parameters while making products robust to variation in the environment and to reduce part to part sensitivity [3]. The Taguchi method is a well-known technique of identifying main machining effects and optimum cutting parameters through the use of orthogonal arrays. This method is widely preferred as it greatly reduces the number of tests required to understand the process even though it cannot account for interaction variables. Alternative toolpath testing in Inconel 718 (IN718) is a time-consuming process and highly costly; IN718 bar stock is approximately thirty times the cost of 6061 aluminum [5]. Thus, the Taguchi Design of Experiment (DoE) approach was chosen to run tests for this work. This method utilizes fractional designs and orthogonal arrays where a large amount of information can

☆ 47th SME North American Manufacturing Research Conference, NAMRC 47, Pennsylvania, USA.

* Corresponding author.
E-mail address: apleta@clemson.edu (A. Pleta).

https://doi.org/10.1016/j.jmapro.2019.03.048
Received 19 November 2018; Received in revised form 21 February 2019; Accepted 8 March 2019
Available online 16 May 2019

Nomenclature

S/N	Signal to noise ratio
F_t	*Tangential force*
F_r	Radial force
F_a	Axial force
R_{cp}	Tool center point radius
R_t	Cutting tool radius
$V_{b\ end}$	Tool flank wear – end
$V_{b\ side}$	Tool flank wear – side
k_t	Tangential cutting force coefficient
k_r	Radial cutting force coefficient
k_a	Axial cutting force coefficient
k_{te}	Tangential edge coefficient
k_{re}	Radial edge coefficient
k_{ae}	Axial edge coefficient
h	chip thickness
$h_{\max}$	maximum chip thickness
t	Time
$\dot{\theta}$	Rotation Rate
$\dot{\phi}$	Nutational rate
a_p	Axial depth of cut
v_{feed}	Translational feed

be gathered from a minimal number of test runs.

Increasing the productivity and efficiency of the trochoidal milling process is critical to allow for better implementation in industry. Currently, when utilizing commercial computer aided machining (CAM) programs there are two groups that programmers can use to optimize the toolpath: (1) tooling parameters and (2) path parameters. The tooling parameters are typically given by manufacturers as the machining speed and the chip load, or feed per tooth. When utilizing trochoidal milling, manufacturers and some CAM programs increase the machining feed rate as an empirically derived percentage, which is typically not derived from the programmer's unique workpiece and tool combination. Alternatively, the programmer can choose to modify the path that the tool follows, which is typically controlled by the stepover distance, the maximum linear distance between successive trochoids or by the maximum radial engagement. Currently the recommendation on which to modify first, tooling or path parameters, is open to the programmer and depends on the CAM vendor and/or tooling supplier.

To better understand the trochoidal milling process in terms of the tooling parameters and path parameters as they relate to machining outputs of resultant cutting force and tool wear, a Taguchi design of experiments is utilized. With this method a limited amount of experiments is run and a general understanding of the machining inputs as they relate to the outputs can be established.

To achieve this objective, the work is organized as follows: In Section 2, the trochoidal tool path equation and developed chip thickness and semi-mechanistic force model are explained. This is followed up with an experimental setup description and test procedures for critical tool path parameter identification and measuring the machining affected zone in Section 3. The results of Taguchi DoE and sensitivity analysis of cutting force and edge force coefficients on machining inputs are discussed in Section 4 while the effect of tool path parameters on machining affected zone depth is discussed in Section 5. Lastly, the conclusion is given in Section 6.

2. Trochoidal tool path construction and experimental setup

2.1. Trochoidal milling toolpath

The trochoidal milling toolpath is a linear path superimposed on the rotational motion of the tool center point as illustrated in Fig. 1. The primary advantage of this toolpath is the increase in tool life when compared to traditional toolpaths; 600% increase in material removed per tool wear unit was reported previously [4]. This is due to the incremental engagement of the tool throughout the machining process. In this work, the trochoidal toolpath is parametrized by three variables: the rotational rate $\dot{\theta}$, the nutational rate $\dot{\phi}$ and the linear feed rate, v_{feed}.

The rotation is defined as positive in the clockwise direction, whereas the nutation is positive in the counter clockwise direction. Both parameters are measured in rad/s and are utilized to model the instantaneous uncut chip thickness, as detailed in a previous work by the authors [6]. These parameters are then converted into CNC interpretable parameters, where $\dot{\theta}$ is the spindle rotational speed and $\dot{\phi}$ is converted into the programmed machining feed rate. Modification of the linear feed rate (v_{feed}) influences the curvature of the trochoid and therefore the distance at which the tool covers, which is incorporated into the machining feed rate as well. The remaining parameters are the tool radius R_t, and the tool center path radius R_{cp}, which is the radius of the arc traversed by tool center point, displayed in Fig. 1 as the dashed line. The mathematical description of the toolpath is defined by Eq. 1, where X_t and Y_t are the cartesian coordinates of the cutter and t is time.

$$\begin{bmatrix} X_t = R_{cp}\cos(\dot{\phi}t) + R_t\cos(\dot{\theta}t) \\ Y_t = R_{cp}\sin(\dot{\phi}t) + R_t\sin(\dot{\theta}t) + v_{feed}t \end{bmatrix} \quad t \in [t_i, t_f] \tag{1}$$

As the linear feedrate term (v_{feed}) grows the path as defined in Eq. 1 departs from the circular approximations that are presented in previous works [7,8]. This is important to note as it adds significant complexity to the instantaneous uncut chip thickness model. Also, in Fig. 1 the nutational speed is effectively chosen much larger than the rotational speed and is responsible for the roulette appearance of the toolpath. This is only for illustrative purposes, whereas in practice the rotational speed is increased to smooth out the roulette shape into a semi-continuous arc, however it is still not geometrically valid to assume a circular shape assumption to describe the path. It should be noted that as the machining speeds and feeds increase, and as the linear distance between the nutations decreases a physical challenge is presented to the CNC machine and its respective controller in terms of its ability accurately reproduce the path as simulated. A controller that can interpret a high-volume of code, especially with advanced look ahead functionality is critical. Acceleration and deceleration simulation and understanding is also vital to increase the viability of the path. As such, the machining parameters presented in this work were chosen to both respect the recommended parameters by the tooling manufacturer and to eliminate the challenges presented as related to acceleration limits of the

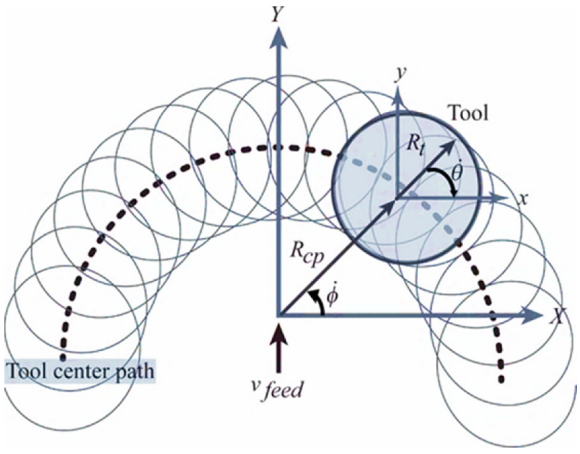

Fig. 1. The trochoidal toolpath comprises three primary machining parameters.

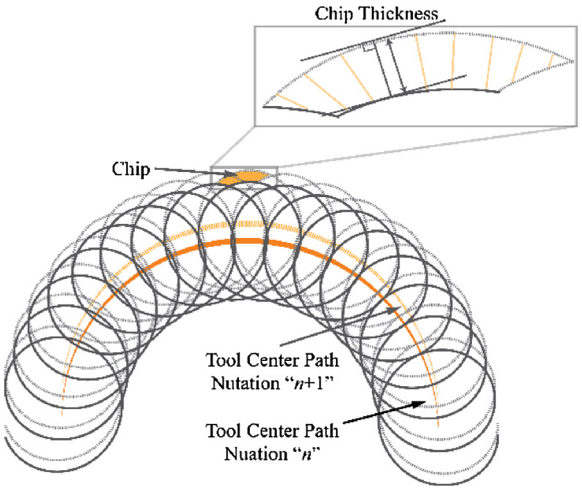

Fig. 2. The chip thickness geometry can be found as the area between two subsequent nutations of the tool. It is measured as the perpendicular distance from the outer manifold to the outer manifold of the previous nutation.

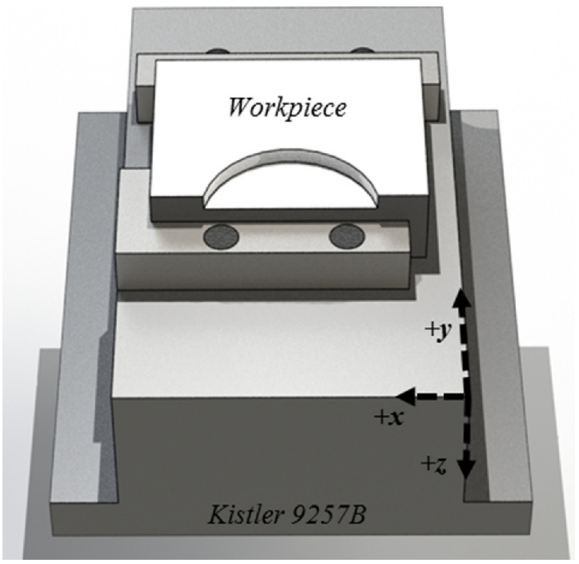

Fig. 3. Test setup with cutting force component directions.

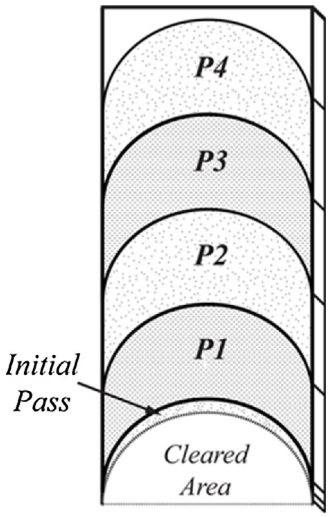

Fig. 4. Wear regions of each test which includes a cleared area, an initial pass of two nutations and four equal volumes of 375 mm^3 material removed.

Table 1
Output response factors for Taguchi L_9 array.

Output Response Factors	Symbol
Tool Wear End (mm)	$Vb_{,end}$
Tool Wear Side (mm)	$Vb_{,side}$
Tangential Edge Coefficient (N/m)	k_{te}
Radial Edge Coefficient (N/m)	k_{re}
Axial Edge Coefficient (N/m)	k_{ae}

Table 2
Trochoidal tool path parameters (inputs).

Path Parameters	Symbol	Level 1	Level 2	Level 3
Rotation rate (RPM)	$\dot{\theta}$	400	600	1200
Nutational rate (rad/s)	$\dot{\phi}$	0.30	0.50	0.70
Axial depth of cut (mm)	a_p	0.50	1.00	0.75
Translational feed (mm)	v_{feed}	0.025	0.050	0.075

Table 3
Control factor parameters for Taguchi L_9 array.

Test Name	$\dot{\theta}$	$\dot{\phi}$	v_{feed}	a_p
T1	1	1	1	1
T2	1	2	2	2
T3	1	3	3	3
T4	2	1	2	3
T5	2	2	3	1
T6	2	3	1	2
T7	3	1	3	2
T8	3	2	1	3
T9	3	3	2	1

machine.

With the toolpath defined, the uncut chip thickness model can then be constructed, which utilizes a numerical approach, as a known closed-form solution does not exist. For the purpose of generality, the chip thickness can be found as the area bound between successive trochoidal paths when tracing the tool tip path of motion as illustrated in Fig. 2. A detailed description of the process can be found in a previous work by the authors [6].

2.2. Cutting force coefficients

This work considers the mechanistic force modeling approach for simulation of cutting forces. With the uncut chip thickness model, the cutting force coefficients and edge force coefficients must first be gathered. Historically, these coefficients are gathered using full radial immersion, which simplifies the chip thickness calculation by reducing the tool entrance and exit angles below 180° [9,10]. In a recent work by the authors it was found that slot milling tests produce coefficients that are not accurate enough to model the process [11]. Therefore, the cutting force coefficients must be gathered from trochoidal milling tests.

To calculate the coefficients, the cutting forces are captured in the global coordinate system of dynamometer and are subsequently decomposed into local tangential F_t, radial F_r, and axial F_a components based on the geometry and rotational angle of the tool using Eq. 2. The cutting forces are then discretised so the exact chip thickness is known at each interval where the coefficients can be calculated using Eq. 3, where a_p is the axial depth of cut and h is the instantaneous chip thickness. The average value for each coefficient is then tabulated across the complete nutation and then reported. Note that, since the forces are gathered over first tool nutation where the cutting edge is still sharp, the edge coefficients (which account for ploughing and frictional effects of the process), represented with a subscript 'e' in Eq.

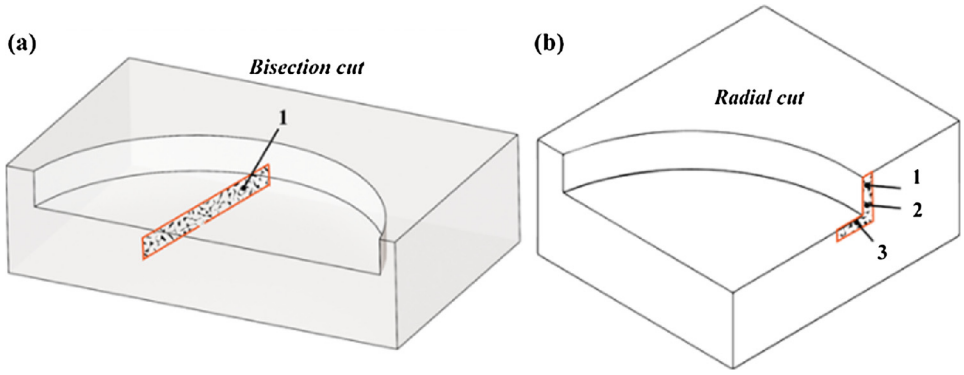

Fig. 5. Samples for MAZ study were cut from the test block in two locations (a) Bisection cut at h_{max} to study axial depth across singular chip thickness (b) Radial cut taken at h_{max} to see MAZ depth in the radial direction and axial direction at the wall.

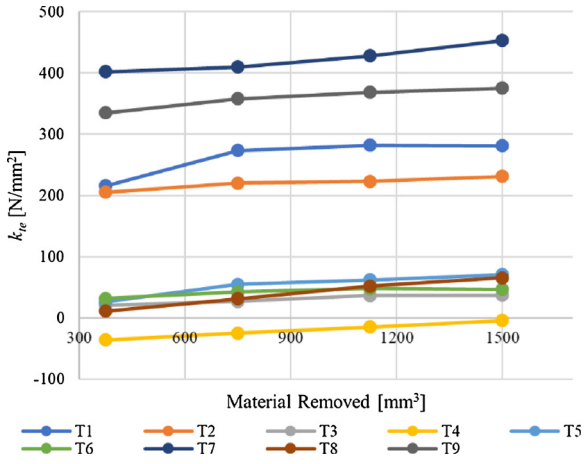

Fig. 6. K_{te} increases linearly with respect to increasing wear state.

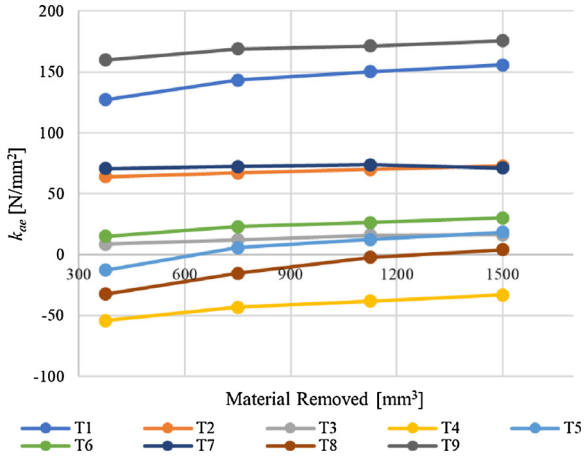

Fig. 7. K_{ae} increases linearly with respect to increasing wear state.

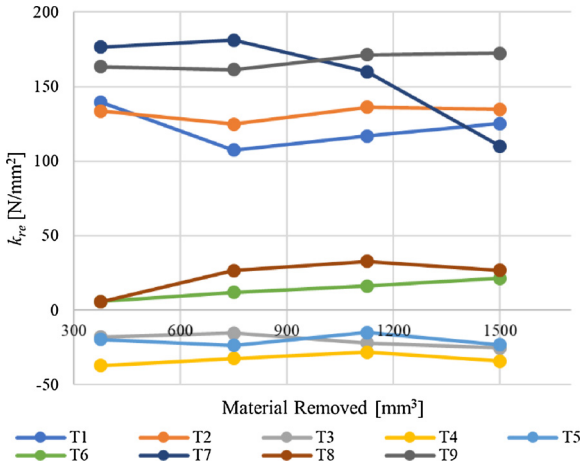

Fig. 8. K_{re} inconsistent behavior with respect to increasing wear state.

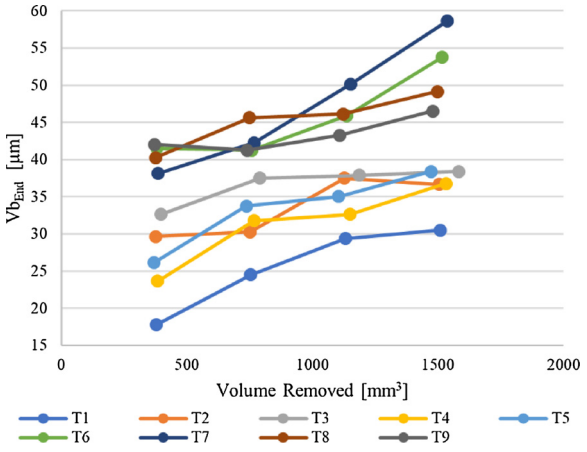

Fig. 9. Flank wear growth across wear states shows continuously increasing values.

4, are assumed to be negligible.

It is assumed that the cutting force coefficient values (k_t, k_r and k_a) found in Eq. 3 remain insensitive to the tool wear at each tool path parameter combinations. With this assumption, the edge coefficients (k_{te}, k_{re} and k_{ae}) can be calculated as described in the following: cutting forces increase rapidly in the milling of nickel-based super alloys due to the formation of tool wear at an increased rate not seen in the milling of more machinable materials such as aluminum or mild steels. The increase in cutting force attributed to wear is captured in the edge effect values (k_{te}, k_{re} and k_{ae}). Therefore, in the difference between simulated force values using the cutting force coefficients at a zero-wear state with no edge effects present, and the measured forces recorded at higher wear states, the edge effects can be found.

For each chip in the cutting process, the peak force was found for both the zero-wear simulation state and the force at an elevated tool wear state. This difference is then used to calculate the edge force coefficients by dividing by the axial depth of cut, a_p. With edge force coefficients values calculated for each chip across a full nutation, the average value is determined and recorded as the edge force coefficients corresponding to the wear state of the tool.

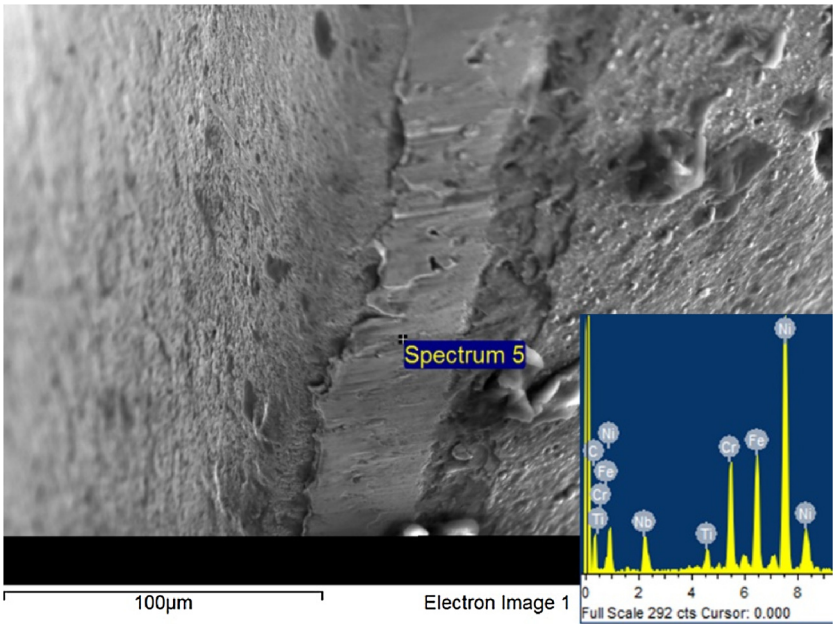

Fig. 10. Built-up-edge on tooling.

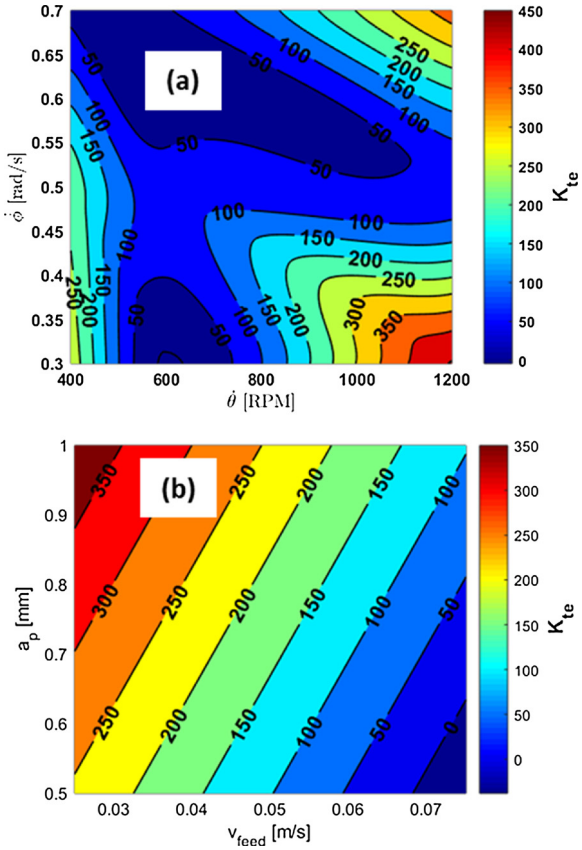

Fig. 11. (a) $\dot{\theta}$ and $\dot{\phi}$ have larger influence on the edge force coefficient (k_{te}) when compared to (b) a_p and v_{feed}.

$$\begin{Bmatrix} F_t \\ F_r \\ F_a \end{Bmatrix} = \begin{bmatrix} -\sin(\theta) & -\cos(\theta) & 0 \\ -\cos(\theta) & \sin(\theta) & 0 \\ 0 & 0 & 1 \end{bmatrix}^{-1} \begin{Bmatrix} F_x \\ F_y \\ F_z \end{Bmatrix} \tag{2}$$

$$k_t = \frac{F_t}{a_p h}, \quad k_r = \frac{F_r}{a_p h}, \quad k_a = \frac{F_a}{a_p h} \text{[at zero wear state]} \tag{3}$$

$$\begin{aligned} F_t &= k_t a_p h + k_{te} a_p \\ F_r &= k_r a_p h + k_{re} a_p \\ F_a &= k_a a_p h + k_{ae} a_p \end{aligned} \tag{4}$$

2.3. The Taguchi method

The Taguchi DoE is designed by creating orthogonal arrays to arrange the factors, so as to avoid interactions. This method has been widely adopted in manufacturing and machining research, in both milling and turning articles. Many of the works in turning focused on finding the optimal parameter set to reach desired level of power usage, tool wear, milling forces and surface finish where speed, feed rate and axial depth of cut where the main influencers of flank wear respectively [12–14]. A full review of the Taguchi method in hard turning applications can be found in the work of Dureja [15]. In the work of Kivak and Meas, the Taguchi L_{18} was used in milling of Hadfield steel, where the flank wear and surface roughness were used as the primary outputs [16]. It was also found in this work that the Taguchi method produces similar results when compared to Response Surface Methodology (RSM). The results also agreed with other works in milling when compared against analysis of variance (ANOVA) approaches which show that these methods can be used interchangeably when utilizing independent input factors [13,17].

In this work, an L_9 orthogonal array was used with four input factors as rotational rate ($\dot{\theta}$), nutational rate ($\dot{\phi}$), translational feed (v_{feed}) and axial depth of cut (a). The primary statistical parameter utilized in the Taguchi method is the signal to noise ratio, denoted as S/N in Eq. 5, which accounts for the mean and standard deviation of the measured responses. There are three categories of S/N ratios that are utilized depending on the results desired and the system under investigation: larger-is-better, smaller-is-better, nominal-is-best. In this investigation, smaller-is-better is chosen as smaller cutting forces are desired coupled with minimal tool wear. The S/N ratio is calculated for each output response factor at each level by using Eq. 5 where n is the number of experiments and y_i is the measured data (i.e. force and tool wear) for the i^{th} experiment, and i is the current test run. The maximum S/N ratio occurs at the point where input parameters provide the optimum solution. ANOVA is then performed to identify the significant input parameters that influence the output factors

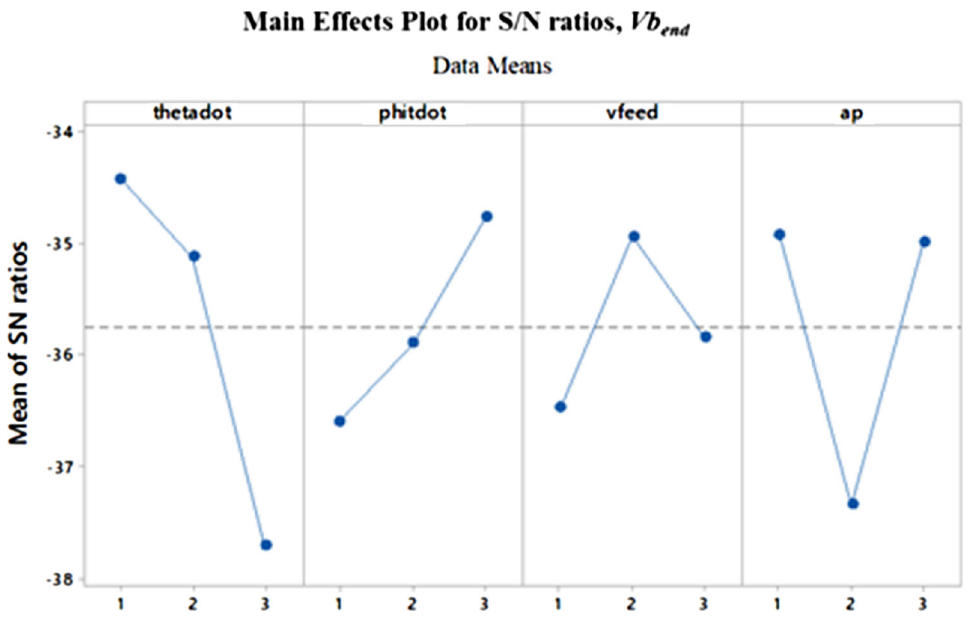

Fig. 12. S/N ratio plot, lower-is-better, showing the effect of input parameters on output Vb_{end}.

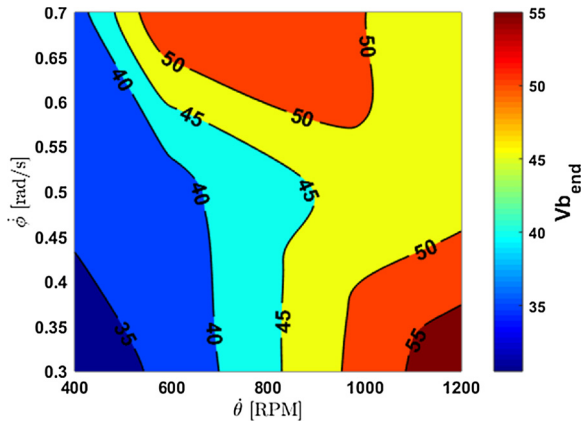

Fig. 13. Effect of $\dot{\theta}$ and $\dot{\phi}$ on Vb_{end}.

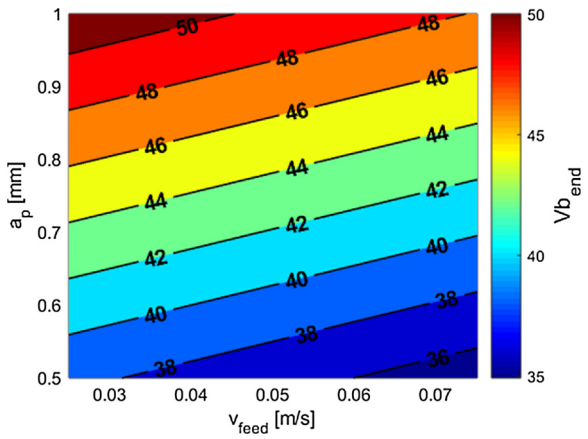

Fig. 14. Effect of v_{feed} and a_p on Vb_{end}.

$$S/N = -10\log\left[\frac{1}{n}\sum_{i=1}^{n} y_i^2\right] \quad (5)$$

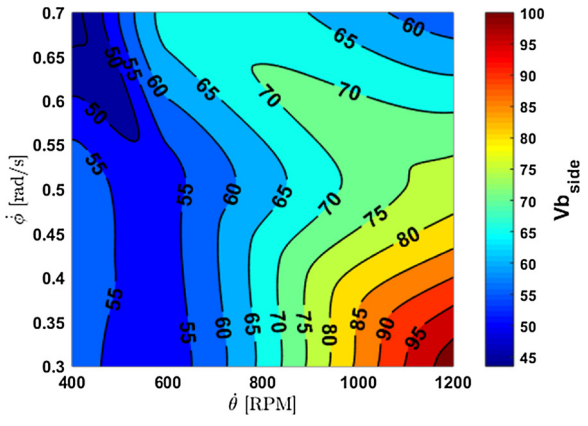

Fig. 15. Effect of $\dot{\theta}$ and $\dot{\phi}$ on Vb_{side}.

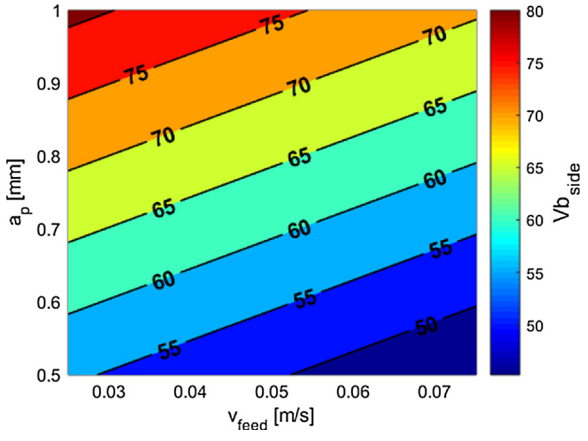

Fig. 16. Effect of v_{feed} and a_p on Vb_{end}.

3. Experimental setup

The experiments were conducted on an Okuma MU-500 V where each IN718 workpiece was mounted to a Kistler 9257B piezoelectric dynamometer to collect cutting force data at 6 kHz sampling frequency, as illustrated in Fig. 3. A two-flute indexable end mill was utilized with

Table 4
MAZ depth test conditions.

Test name	Nutation rate $\dot{\phi}$ [rad/s]	Rotation rate $\dot{\theta}$ $\dot{\theta}$ [rpm]	# of chips	Max chip thickness h_{max} [mm]
M1	0.7	400	58	0.206
M2	0.3	1200	419	0.048

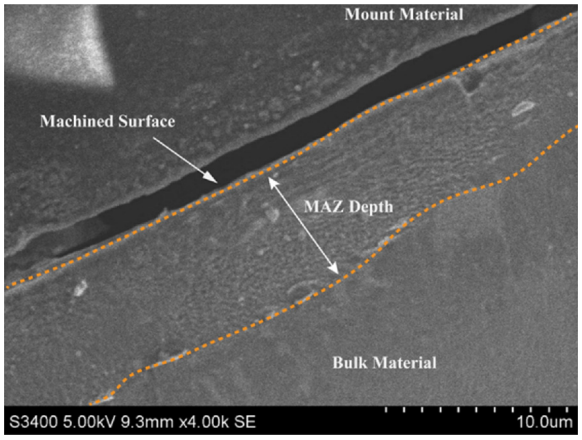

Fig. 17. The MAZ is measured from the machined surface of the material to the boundary of deformed grains where the bulk material resumes.

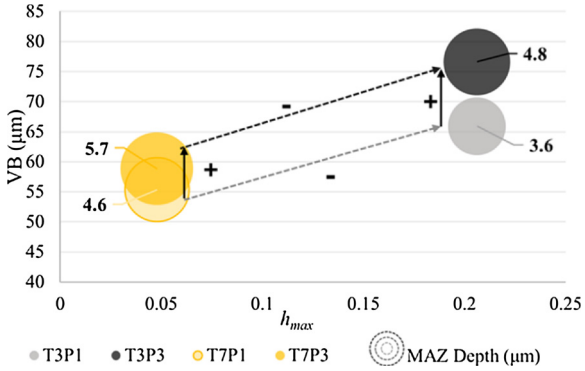

Fig. 18. The axial MAZ depth near the surface of the part increases with Vb_{end} across both test conditions where the depth is represented by the area of each bubble.

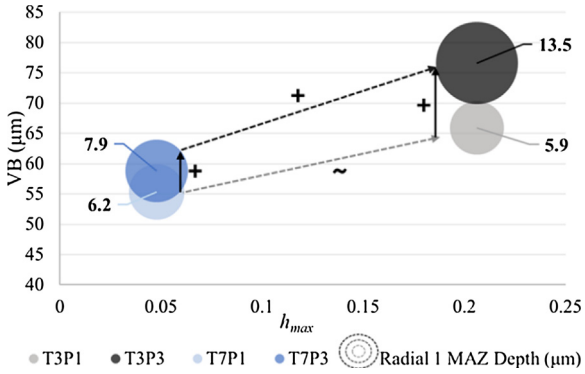

Fig. 19. The radial MAZ depth near the surface of the part increases with VB across both test conditions where the lower nutational rate condition produces the smaller radial MAZ depth due to reduced milling forces where the depth is represented by the area of each bubble.

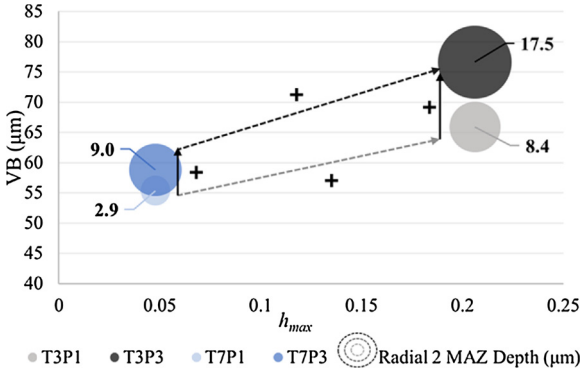

Fig. 20. The radial MAZ when measured at the bottom of the cut, near to where the tool nose is cutting, the radial MAZ increases with VB across both test conditions with the larger increase in MAZ depth when compared to measurement location 1 where the depth is represented by the area of each bubble.

Sandvik Coromant Coromill R390-11T308M-PM-1130 carbide inserts with TiAlN coating. The tooling exhibits a lead angle γ_L of 90°, axial rake angle γ_A of 12.4°, and radial rake angle γ_R of 2.5° with a tool diameter of 15.875 mm. Flood coolant was utilized for all tests at a concentration of 6.5% as recommended by the supplier (Fortech FT2005).

To investigate the cutting forces at elevated wear states each test condition is divided into five individual test runs. The first test pass (initial pass) is recorded after the material is removed from the workpiece by a separate tool to produce the part geometry where the initial pass will pass through the exact geometric definition of the toolpath as illustrated in Fig. 4 (P1 through P4 in Fig. 4). The initial pass contains two full nutations of the tool and produces a negligible amount of tool wear, negating the edge force coefficients. The force captured in the initial pass will then be used to calculate the cutting force coefficients (k_t, k_r and k_a) given in Eq. 3. The measured cutting forces in the subsequent passes P1 through P4, are affected by development of tool flank wear and therefore the tool wear is measured after removing consistent volume of material (= 375 mm^3). This way the wear state can be correlated with the volumetric removal. The worn tool is utilized to machine all volumes and a new tool is used for each test condition.

3.1. Trochoidal path experiments

The output response factors in this study consisted of the average tool flank wear end, ($V_{b,\ end}$), average flank wear side ($V_{b,\ side}$), along with tangential, (k_{te},) radial, (k_{re}) and axial, (k_{ae}) edge force coefficients tabulated in Table 1. Input parameters consists of trochoidal milling path parameters are given in

Table 2. The input parameters were selected to cover a wide range of operational parameters including the tooling manufacturer's recommendations. It should be noted that the upper limit of cutting parameters was finalized after running multiple tests to failure. The L_9 Taguchi DoE is given in Table 3.

3.2. Machining affected zone experiments

Images of Machining Affected Zone (MAZ) in radial and axial cutting directions was taken with a Hitachi S3400 Scanning Electron Microscope (SEM) at 4.00k magnification. The specimens were cut from test blocks after both P1 and P3 volume states using wire electro-discharge machine. Each sample was mounted, polished and etched using Marble's reagent to reveal the grain structure. For each volume state, two samples were created to gain insight into the influence of the machining conditions and the tool wear state on the depth of the MAZ as illustrated in Fig. 5. The bisection cut is perpendicular to the trochoidal arc where the chip thickness reaches a maximum giving insight

into the axial MAZ depth at h_{max} where a single measurement location was examined (see Fig. 5a).

The second sample section is in the radial cut (Fig. 5b) which allows the MAZ depth in both the radial and axial directions to be measured. The radial MAZ depth is important to investigate as it may allow for optimization of the trochoidal stepover feed ($v_{feed}t$), therefore the tool can avoid cutting in the work-hardened regions of the material. Two measurement locations are investigated for the radial direction, with the first near the top of the workpiece (see location 1 in Fig. 5(b)), closest to the uncut material, and the second at the bottom of the wall (see location 2 in Fig. 5(b)) where the tool nose radius is removing the material. A third point is also investigated here to allow for measurement in the axial direction at the wall of the part.

4. Experimental results

To gain a general understanding of the dependence of edge force coefficients on the tool wear state, they were calculated for each condition after each test pass group (P1-P4). In Fig. 6, it can be seen that k_{te} has a generally increasing trend throughout the wear states across all parameters. This widely known phenomenon occurs due to the changing geometry of the cutting tool as it wears. The cutting mechanism changes from a primarily shear type with a sharp edge and moves into a ploughing state, where friction, pressure and temperature increase in the cutting zone. This behaviour was also observed in k_{ae} where the effective length of the tool decreases throughout the wear states and also dulls, which further increases the ploughing and friction loads as shown in Fig. 7. The radial edge coefficient, k_{re}, diverges from this continuously increasing trend and instead presents varying trends across parameters, which contrast each other as seen in Fig. 8. This behaviour in contrast to development of flank wear behaviour shown in Fig. 9 where it continuously increases across each wear state and all test conditions. It is believed that the inconsistent behaviour in k_{re} is due to the continuous built-up edge formation and breakage. Due to the low thermal conductivity of IN718, the heat will accumulate at the tool tip interface which leads to high cutting temperature. The high temperature excites the adhesive wear formation and therefore creates a steady formation and breakage of workpiece build up material on the tool. This built up material can act as a boon or a ban based on the operating conditions. The variations along k_{re} can thus be attributed to build up edge formations which is confirmed through scanning electron microscopy results shown in Fig. 10.

Taguchi analysis was conducted on the obtained data. As previously mentioned, the output response factors were the edge force coefficients and flank wear end/side. The goal of this process was to efficiently understand the basic system where the most detrimental input parameters of the process would be identified for a full DoE. A surface plot for each edge force coefficient was generated to study the dominant influencing parameters Fig. 11, where the edge effects were standardized between 0 and 1 to allow for comparison. This analysis was done after the fourth wear state, P4, to understand the behaviour at the maximum amount of wear and the largest amount of difference between new tool and highly dull tool states. The translational feed, v_{feed}, and a_p show similar behaviour across all edge force coefficients, where the maximum values are found at the low a_p and v_{feed} followed by the level-3 a_p and level-2 v_{feed}.

As shown in Fig. 11, $\dot{\theta}$ and $\dot{\phi}$, create the largest variation in edge force coeffcients, when compared to a_p and v_{feed}. The minimum values occur at level-2 of $\dot{\theta}$ and $\dot{\phi}$ and $\dot{\theta}$ for all coefficients which corresponds to the mid-range of chip thickness values and number of chips. This demonstrates that there is a balance to be found between the number of chips and their thicknesses, which is found in industry under the term *chip-thinning*. Too small of a chip creates high wear as there is more rubbing than cutting whereas too large of a chip increases cutting forces and tool wear, so an optimum solution is required. With the largest variations created by $\dot{\theta}$ and $\dot{\phi}$, it can be conculuded that these are the main parameters affecting the edge force coeffcient k_{te}. To undertand if these parameters are masking the influnece of flank wear on the edge coefficients, S/N ratio calculations were completed and illustrated in Fig. 12. Here it shows that $\dot{\theta}$ and $\dot{\phi}$ are the first and third most influential parameters affecting tool wear end. This confirms that rotational speed is a main factor influencing the tool wear. According to Fig. 12, While a_p is highly influential, its effect on the edge force coefficients (see Fig. 11(b) as an example) is so low that its effect can be considered negligible.

The effect of pairs of $\dot{\theta}$ and $\dot{\phi}$ and a_p and v_{feed} on tool wear end (Vb_{end}) and tool wear side (Vb_{side}) were also investigated and shown in Figs. 13–14 it can be seen that the minimum of Vb_{end} occurs by selection of the input parameters $\dot{\theta}$ = 500 rpm; $\dot{\phi}$ = 0.3 rad/s, v_{feed} = 0.08 m/s, and a_p = 0.75 mm. From Figs. 15 and 16, it can be seen that the minimum of Vb_{side} occurs by selection of present for the input parameters $\dot{\theta}$ = 750 rpm; $\dot{\phi}$ = 0.6 rad/s; v_{feed} = 0.08 m/s, and a_p = 0.75 mm.

Furthermore, the combined effect of all parameters should be considered to minimize both tool wear end/side and edge force coefficients. Here, the optimal cutting condition was identified as $\dot{\theta}$ = 400 rpm, $\dot{\phi}$ = 0.7 rad/s, v_{feed} = 0.075 m/s, and a_p = 0.50 mm.

5. Machining affected zone depth study

To understand the interaction between the trochoidal milling toolpath and MAZ depth of IN718 two additional test conditions were tested which took the maximum nutational rate from the previous test sets and combined it with the minimum rotation rate and vice versa. Through this combination the test with the largest chip thickness (see M1 in Table 4), created the lowest number of chips and test with the minimum chip thickness (M2 in Table 4) produced the maximum number of chips.

Measurement of the MAZ depth was completed using the same methodology used in tool wear measurement, where five locations were measured for each location and the average value is reported. Each measurement is the linear distance from the machined surface to the boundary of deformed grains, bounded by the dashed line in Fig. 17, where the deformation transitions into the bulk material.

To establish a baseline of understanding of the axial depth of the MAZ, the bisection sample (Fig. 5(a)) is examined at the location of *hmax*. As illustrated in Fig. 18 the MAZ depth increases with Vb_{end} across both machining conditions, where the depth is represented by the area of each bubble. This behaviour is due to the increasing axial forces imparted by the tool as it wears, where the axial force increases by 16% from M1P1 to M1P3, where M2 sees an increase of 26% from the low to high wear state. Moving from the low chip thickness condition (test M2) to the high chip thickness condition (test M1), the MAZ depth decreases. This increase depth cannot be attributed to axial or resultant cutting force, instead, this occurs due to the increase in plastic deformation which occurs at increased feed rates. These results are in agreement with previous work, where this same trend is identified [18,19]. This behavior was also found at location 3 for the radial cut illustrated in Fig. 5(b).

In the radial direction, the influence of tool wear manifests itself as it does in the axial direction, as the tool wear increases, the depth of the MAZ increases across both conditions. At measurement location 1 in Fig. 5(b), near the machined surface, the radial depth increases as *hmax* increases for the higher wear state passes (P3), whereas a slight decrease occurs at the lower wear state, as illustrated in Fig. 19. The trend in this direction does not follow the results in the axial direction, where the lower nutational rate conditions produce higher MAZ depths. To explain this, the resultant force of the tangential and radial directions is found to be the primary reason of radial depth increase as the M1P1 condition produces a resultant force 55% higher than M2P1 and the higher wear condition, M1P3, 63% larger than M2P3.

Moving to the second measurement location further from the

surface, near to where the tool nose radius is doing the cutting, the radial MAZ depth for both M1 conditions is larger when compared to M2. At the low wear state, instead of a minor reduction when moving from M2 to M1, this location produces a drastic increase from 2.9 μm to 8.4 μm as illustrated in Fig. 20. The larger increase between the conditions at this depth can be attributed to the mechanics of the cutting, where cutting pressures are higher in the tool nose radius area when compared to the location higher on the tool.

6. Conclusion

The Taguchi method was utilized in this paper to understand the influence of machining parameters and tool path parameters on machining outputs in terms of machining force and tool flank wear. It was found that the nutational rate and rotational rate have the largest interactions with both cutting forces and tool flank wear. The depth of the machining affected zone in both radial and axial directions was also investigated in this study, where it was found that chip thickness and tool wear increase the depth of the plastically deformed and elongated grains in both the radial and axial orientations. The results set the stage for future work into the trochoidal milling toolpath. The main advantage of this understanding is to better CAM toolpath generation algorithms, where programmers will be able to reach optimum machining conditions more efficiently and the CAM algorithms will respect material subsurface alterations and residual stresses.

Future work will include an investigation into the dynamics of this toolpath method as it relates to acceleration limits of axes and CNC controllers along with an investigation into residual stresses. This work also sets the stage for a full design of experiments for trochoidal milling to better understand the machining parameters influence on tool life, milling forces and workpiece material affects.

Acknowledgements

The authors would like to thank Okuma America for their partnership in the supply of the MU-5000V to Clemson University for testing and validation of results. The authors would also like to thank the National Science Foundation for support of this work under Grant No. 1760809. Any opinions, findings, and conclusions or recommendations expressed in this material are those of the authors and do not necessarily reflect the views of the National Science Foundation.

References

[1] Gao Y, Ma J, Jia Z, Wang F, Si L, Song D. Int J Adv Manuf Technol 2016;84:1757–67.
[2] Sui S, Li Y, Shao W, Feng P. Int J Adv Manuf Technol 2016;85:1553–64.
[3] Akhavan Niaki F, Pleta A, Mears L. Int J Adv Manuf Technol 2018;97:641–56.
[4] Pleta A, Ulutan D, Mears L. American Society of Mechanical EngineersASME 2014 Int. Manuf. Sci. Eng. Conf. Collocated with JSME 2014 Int. Conf. Mater. Process. 42nd North Am. Manuf. Res. Conf.2014. ASME 2014 Int. Manuf. Sci. Eng. Conf. Collocated with JSME 2014 Int. Conf. Mater. Process. 42nd North Am. Manuf. Res. Conf. 2014. p. V002T02A058-V002T02A058.
[5] Akhavan Niaki F, Ulutan D, Mears L. J Manuf Sci Eng 2016;138.
[6] Akhavan Niaki F, Pleta A, Mears L. Int J Adv Manuf Technol 2018;97:641–56.
[7] Otkur M, Lazoglu I. Int J Mach Tools Manuf 2007;47:1324–32.
[8] Kardes N, Altintas Y. J Manuf Sci Eng 2007;129:21.
[9] Jayaram S, Kapoor SGG, Devor RE. Int J Mach Tools Manuf 2001;41:265–81.
[10] Gonzalo O, Beristain J, Jauregi H, Sanz C. Int J Mach Tools Manuf 2010;50:765–74.
[11] Pleta A, Niaki FA, Mears L. Procedia Manuf 2018;26:570–9.
[12] Dureja JS, Singh R, Bhatti MS. Prod Manuf Res 2014;2:767–83.
[13] Krishna Madhavi S, Sreeramulu D, Venkatesh M. Mater Today Proc 2017;4:1937–46.
[14] Sonawane SA, Kulkarni ML. J King Saud Univ - Eng. Sci 2018;30:250–8.
[15] Dureja JS, Gupta VK, Sharma VS, Dogra M, Bhatti MS. A review of empirical modeling techniques to optimize machining parameters for hard turning applications. Proc Inst Mech Eng Part B: J Eng Manuf 2016;230(3):389–404.
[16] Kivak T. Meas J Int Meas Confed 2014;50:19–28.
[17] Vishnu Vardhan M, Sankaraiah G, Yohan M, Jeevan Rao H. Mater Today Proc 2017;4:9163–9.
[18] Touazine H, Akab J, Jahazi M, Tahan A, Jomaa W, Bocher P. Int J Adv Manuf Technol 2017;93:3705–12.
[19] Pawade RS, Joshi SS, Brahmankar PK, Rahman M. J Mater Process Technol 2007;192–193:139–46.